Pressure-induced unconventional superconductivity in the heavy-fermion antiferromagnet $CeIn_3$: An ^{115}In-NQR study under pressure

S. Kawasaki,[1,*] M. Yashima,[1] Y. Kitaoka,[1] K. Takeda,[2] K. Shimizu,[3] Y. Oishi,[4] M. Takata,[4] T. C. Kobayashi,[5] H. Harima,[6] S. Araki,[7] H. Shishido,[7,†] R. Settai,[7] and Y. Ōnuki[7]

[1]*Department of Materials Engineering Science, Graduate School of Engineering Science, Osaka University, Toyonaka, Osaka 560-8531, Japan*

[2]*Department of Electrical and Electronic Engineering, Muroran Institute of Technology, Mizumoto, Muroran, 050-8585, Japan*

[3]*KYOKUGEN, Research Center for Materials Science at Extreme Conditions, Osaka University, Toyonaka, Osaka 560-8531, Japan*

[4]*Japan Synchrotron Radiation Research Institute, Sayo, Hyogo 679-5198, Japan*

[5]*Department of Physics, Faculty of Science, Okayama University, Okayama 700-8530, Japan*

[6]*Department of Physics, Kobe University, Nada, Kobe 657-8501, Japan*

[7]*Department of Physics, Graduate School of Science, Osaka University, Toyonaka, Osaka 560-0043, Japan*

(Received 6 July 2007; revised manuscript received 18 September 2007; published 14 February 2008)

We report on pressure-induced unconventional superconductivity (SC) in the heavy-fermion (HF) antiferromagnet $CeIn_3$ by means of nuclear-quadrupole-resonance (NQR) studies conducted under a high pressure. The temperature (T) and pressure (P) dependences of the In-NQR spectra have revealed a first-order quantum-phase transition (QPT) from antiferromagnetism (AFM) to paramagnetism (PM) at a critical pressure $P_c = 2.46$ GPa at which AFM disappears with a minimum value of $T_N(P_c) = 1.2$ K. High-energy x-ray scattering measurements under P show a progressive decrease in the lattice density without any change in the crystal structure, whereas an increase in the NQR frequency (ν_Q) indicates an increase in the hybridization between $4f$ electrons and conduction electrons, which stabilizes the HF-PM state. This competition between the AFM phase where T_N is reduced and the formation of the HF-PM phase triggers the first-order QPT at $P_c = 2.46$ GPa. Despite the lack of an AFM quantum critical point in the P-T phase diagram, we highlight the fact that unconventional SC occurs in both phases of AFM and PM. The measurements of the nuclear spin-lattice relaxation rate $1/T_1$ in the AFM phase have provided evidence for the uniformly coexisting AFM+SC phase. Remarkably, the significant increase in $1/T_1$ upon cooling in the AFM phase has revealed the development of low-lying magnetic excitations down to T_c in the AFM phase; it is indeed relevant to the onset of the uniformly coexisting AFM+SC phase. In the HF-PM phase where AFM fluctuations are not developed, $1/T_1$ decreases without the coherence peak just below T_c, followed by a power-law-like T dependence that indicates an unconventional SC with a line-node gap. Remarkably, T_c has a peak around P_c in the HF-PM phase as well as in the AFM phase. In other words, an SC dome exists with a maximum value of $T_c = 230$ mK around P_c, indicating that the origin of the pressure-induced HF SC in $CeIn_3$ is *not relevant to AFM spin fluctuations but to the emergence of the first-order QPT* in $CeIn_3$. These phenomena observed in $CeIn_3$ should be understood in terms of the first-order QPT because these new phases of matter are induced by applying P. When the AFM critical temperature is suppressed at the termination point of the first-order QPT, $P_c = 2.46$ GPa, the diverging AFM spin-density fluctuations emerge at the critical point from AFM to PM. The results with $CeIn_3$ leading to a new type of quantum criticality deserve further theoretical investigations.

DOI: 10.1103/PhysRevB.77.064508 PACS number(s): 74.25.Dw, 71.27.+a, 75.30.Kz, 76.60.−k

I. INTRODUCTION

In f-electron-based compounds, the hybridization between f electrons and conduction electrons results in interesting physical phenomenon via the formation of a heavy-fermion (HF) state at low temperatures.[1] In particular, since the discovery of the first HF superconductor $CeCu_2Si_2$ in 1979,[2] HF superconductivity (SC) has attracted remarkable attention as a candidate for understanding the mechanism for unconventional SC discovered in strongly correlated electron systems (SCESs).[3] A common type of SC is based on bound electron pairs coupled via the lattice vibration.[4] However, the SC in SCESs including many HFs, cuprates, and organic superconductors appears to have another binding force that forms Cooper pairs via electron-electron correlation. In particular, a number of studies on f-electron compounds revealed that an unconventional SC arises at or close to a second-order quantum-phase transition (QPT)—i.e., the quantum critical point (QCP), where the magnetic order disappears at $T=0$ as a function of lattice density due to the application of hydrostatic pressure (P). In other words, near the magnetic order, the magnetic interaction between electron spins can mediate attractive interactions between the charge carriers. Phase diagrams have been obtained for antiferromagnetic HF compounds such as $CePd_2Si_2$ (Refs. 5–7), $CeIn_3$ (Refs. 5 and 7–11), and $CeRh_2Si_2$(Refs. 12 and 13); these are schematically shown in Fig. 1(a). Significantly different behavior, schematically shown in Fig. 1(b), has been observed in the archetypal HF superconductor $CeCu_2Si_2$ (Refs. 2 and 14–17) and the more recently discovered $CeRhIn_5$ (Refs. 18–20). Although both compounds have demonstrated an analogous behavior relevant to a magnetic QCP, it is noteworthy that an associated superconducting region extends to higher densities than in other compounds;

 ©2008 The American Physical Society

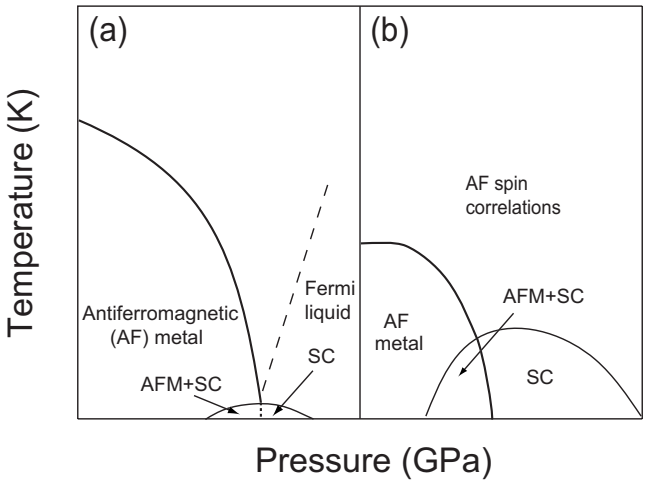

FIG. 1. Schematic phase diagrams of Ce-based heavy-fermion compounds: (a) for $CePd_2Si_2$ (Refs. 5–7), $CeIn_3$ (Refs. 5 and 7–10), and $CeRh_2Si_2$ (Refs. 12 and 13); the dashed line indicates the crossover; (b) for $CeCu_2Si_2$ (Refs. 2 and 14–17) and $CeRhIn_5$ (Refs. 18–20).

their T_c value reaches its maximum away from point at which antiferromagnetism (AFM) is achieved.[14,15,19] Most interestingly, previous nuclear-quadrupole-resonance (NQR) studies have revealed that AFM and SC coexist microscopically and that SC does not exhibit any trace of a line-node gap opening in the low-lying excitations below T_c that are characteristic of the HF superconductors reported thus far.[17,21,22]

Recently, it has been demonstrated by an extensive NQR study conducted under a high pressure that the P-T phase diagram at zero magnetic field ($H=0$) in $CeRhIn_5$ is characterized by a tetracritical point separating the pure AFM phase, the uniformly coexisting phase of AFM+SC, the SC phase, and the paramagnetic (PM) phase. Note that the AFM phase transition occurs inside the SC below T_c when a tetracritical point is exceeded.[20] This result has revealed a close relationship between AFM and SC—both phases may be mediated by the same magnetic interaction. In contrast, the two superconducting domes have been reported to be a function of P in the case of $CeCu_2(Si_{1-x}Ge_x)_2$ (Ref. 23); however, the origin of SC in HF compounds is still a topical issue. One dome (SC1) is formed around the AFM QCP, whereas the other (SC2) emerges in the HF state without any indication of AFM spin fluctuations because the system is still far from the point of the AFM QCP. Interestingly, the maximum T_c value in SC2 as the function of P is higher than that in SC1 in the case of $CeCu_2(Si_{1-x}Ge_x)_2$. Although the possible origins of SC2 are not yet known, a new type of pairing mechanism, besides AFM spin fluctuations, has been suggested for mediating the Cooper pairs in HF systems. For instance, valence fluctuations of Ce ions may be responsible for the onset of SC2 via the increase in hybridization between the Ce 4f electrons and conduction electrons.[23–26] Two SC domes have also been suggested in the case of $CeRh_{1-x}Ir_xIn_5$.[27–30] These results suggest that there are still underlying issues that remain to describe rich phases of matter appearing in the antiferromagnetic HF systems under P.

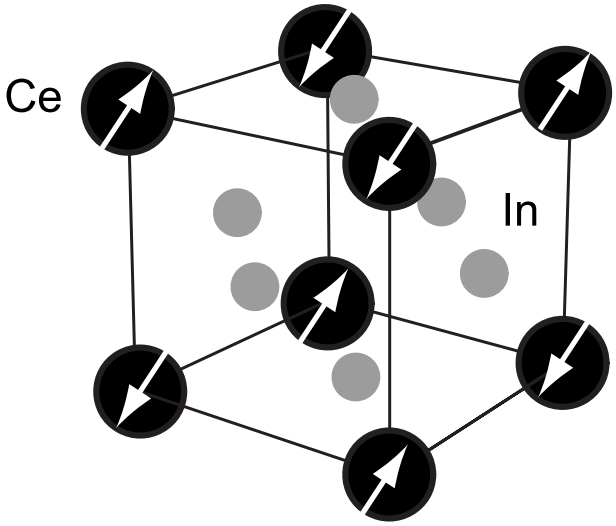

FIG. 2. Crystal and spin structures of $CeIn_3$ below T_N.

As shown in Fig. 2, $CeIn_3$ is formed in the cubic $AuCu_3$ structure and orders antiferromagnetically below the Néel temperature $T_N=10.2$ K at an ambient pressure ($P=0$). It has an ordering vector $\mathbf{Q}=(1/2,1/2,1/2)$ (Ref. 31) and Ce magnetic moment $M_{AFM}\sim 0.5\mu_B$, which were determined by NQR measurements[32,33] and a neutron-diffraction experiment on single crystals,[34] respectively. The resistivity measurements of $CeIn_3$ revealed the P-T phase diagram of the AFM and SC—T_N decreases with increasing P, and on almost near the point where AFM is achieved, SC emerges in a narrow P range of approximately 0.5 GPa, thereby exhibiting a maximum value of $T_c\sim 200$ mK at around $P_c=2.5$ GPa where AFM disappears.[5,7–10] A non-Fermi-liquid behavior was suggested from the $T^{3/2}$ dependence of resistivity within the framework of spin fluctuations theory[35] in the narrow P and T ranges around P_c. Then, it was inferred that magnetic fluctuations can mediate spin-dependent attractive interactions between the charge carriers in $CeIn_3$.[5,7–10]

Previous NQR studies have revealed a systematic change in the magnetic character through the measurements of the nuclear-spin-lattice relaxation rate $1/T_1$ of the ^{115}In-NQR under P.[11,36–38] The localized magnetic character of $4f$ magnetic moments is robust up to $P=1.9$ GPa. The characteristic temperature T^*, below which the system crosses over to an HF regime, increases dramatically with further increase in P. As a result, the HF state becomes stable due to the increase in T^* as P increases beyond P_c. The measurements of $1/T_1$ and ac susceptibility (χ_{ac}) at $P=2.65$ GPa until $T=50$ mK provided the first evidence of an unconventional SC at $T_c=95$ mK in $CeIn_3$,which arises in the fully established HF state below $T_{FL}=5$ K.[38] The phase separation into the AFM and PM phases in $CeIn_3$ is evidenced from the observation of two kinds of NQR spectra around P_c.[11] Nevertheless, it was demonstrated that SC in $CeIn_3$ occurs in both phases at $P=2.43$ GPa, where the maximum value of $T_c^{max}=230$ mK is observed for the PM phase. Remarkably, SC uniformly coexists with AFM below $T_c=190$ mK.[11] Furthermore, a first-order QPT was suggested from a possible phase separation into the AFM and HF-PM phases near P_c. However, since

the possibility that this phase separation near P_c is due to an inevitable distribution of P inside the pressure cell cannot be ruled out, we cannot conclude whether QPT is of first or second order. In this paper, through extensive In-NQR studies, we provide insights into a P-T phase diagram in $CeIn_3$ and into the origin of the unconventional SC that emerges in the vicinity of a first-order QPT transition from the AFM phase to the HF-PM phase.

II. EXPERIMENTAL PROCEDURES

High-quality single crystals of $CeIn_3$ were grown by the Czochralski method. They were moderately crushed into grains so that rf pulses can easily penetrate into the samples. However, in order to avoid crystal distortions, the grain diameters were kept larger than 100 μm. A small piece of $CeIn_3$ cut from the same batch as the sample used in the present work exhibited zero resistance in a range $P=2.2-2.8$ GPa,[9] which is in good agreement with the previous reports.[5,7,10] An ^{115}In-NQR spectrum was obtained by plotting the spin-echo intensity as a function of frequency. In order to detect an internal magnetic field associated with the onset of AFM around P_c, the NQR spectrum for the $1\nu_Q$ $(\pm 1/2 \leftrightarrow \pm 3/2)$ transition was precisely obtained by the Fourier transform method of a spin-echo signal. Under the condition that the NQR spectra result from both phases of AFM and PM in the vicinity of P_c, each volume fraction was estimated from the NQR intensity $I(0)$ for the $1\nu_Q$ transition, which was precisely estimated through a fitting to $I(t)=I(0)\exp(-t/T_2)$, where T_2 is the nuclear spin-spin relaxation time. The ^{115}In-NQR T_1 was measured by the conventional saturation-recovery method in a range of $T=0.05-70$ K. The $2\nu_Q$ $(\pm 3/2 \leftrightarrow \pm 5/2)$ and $1\nu_Q$ $(\pm 1/2 \leftrightarrow \pm 3/2)$ transitions were used for the T_1 measurement above and below $T=1.4$ K, respectively. The high-frequency χ_{ac} was measured by using an *in situ* NQR coil.[21] Hydrostatic pressure was applied by utilizing a NiCrAl-BeCu piston-cylinder-type clamping cell filled with Si-based organic liquid as a pressure-transmitting medium.[39] In order to calibrate the pressure at low temperatures, the shift in T_c of the Sn metal under P was measured by the conventional four-terminal resistivity measurement. To reach the lowest temperature of 50 mK, a ^{3}He-^{4}He dilution refrigerator was used.

The ^{115}In-NQR spectra in the PM state at $T=77$ K and $P=0$ are shown in the top of Fig. 3(a) where four transitions are observed at different frequencies $\nu=n\nu_Q$ for $n=1$, 2, 3, and 4. Here, ν_Q is defined by the NQR Hamiltonian $\mathcal{H}_Q=(h\nu_Q/6)[3I_z^2-I(I+1)+\eta(I_x^2-I_y^2)]$, where η is the asymmetry parameter of the electric field gradient. Note that $\nu_Q=9.61$ MHz and $\eta=0$ at $P=0$. Since the full width at the half maximum (FWHM) for the $1\nu_Q$-NQR spectrum is quite sharp at 60 kHz, the sample that is used here is confirmed to be of high quality. Under the condition that the AFM order set in, the Hamiltonian of the ^{115}In nuclei is replaced by $\mathcal{H}_{AFM}=-\gamma\hbar\vec{I}\cdot\vec{H}_{int}+\mathcal{H}_Q$, where $\vec{H}_{int}=(H_\perp,0,H_\parallel)$ is an internal magnetic field associated with the onset of AFM order. In the case of $CeIn_3$, $H_\parallel$ is canceled at the position of the In site. Hence, the onset of AFM order for $CeIn_3$ is identified from the splitting of the $1\nu_Q$ spectrum and the frequency shift of the other spectra due to the appearance of $H_\perp$.

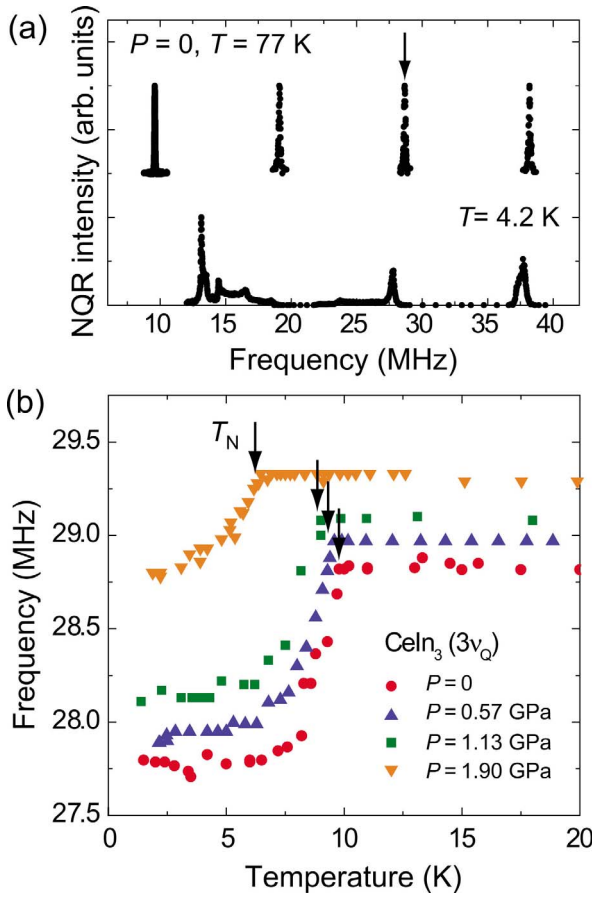

FIG. 3. (Color online) (a) NQR spectra for $CeIn_3$ above and below $T_N=10.2$ K at $P=0$. The solid arrow indicates the position of the $3\nu_Q$ transition. (b) The T dependence of the peak of the $3\nu_Q$ spectrum in a range of $P=0-1.90$ GPa. The solid arrows point to T_N.

In fact, the NQR spectra at $T=4.2$ K below T_N are indicated at the bottom of Fig. 3(a), revealing a significant change due to the presence of $H_\perp$. Note that the $3\nu_Q$ and $4\nu_Q$ spectra remain extremely sharp even below T_N, which guarantees that H_{int} is homogeneously determined at all the In sites below T_N. These results are consistent with the previous NQR measurements.[32,33] Extensive analyses of these spectra as the functions of T and P enable us to determine $T_N(P)$ and the value of the antiferromgnetically ordered moment $M_{AFM}(T,P)$ as functions of P and T for $CeIn_3$ even in close proximity to P_c.

The pressure dependence of the unit cell volume at low temperature was measured by powder x-ray diffraction experiments using synchrotron radiation in SPring-8 BL10XU. The experiment was carried out by using a He-gas-driven diamond-anvil cell. The pressure medium was methanol-ethanol mixture. The pressure was determined by the ruby fluorescence method. The lattice parameter were refined by the Rietveld method using the RIETAN-2000 program.[40]

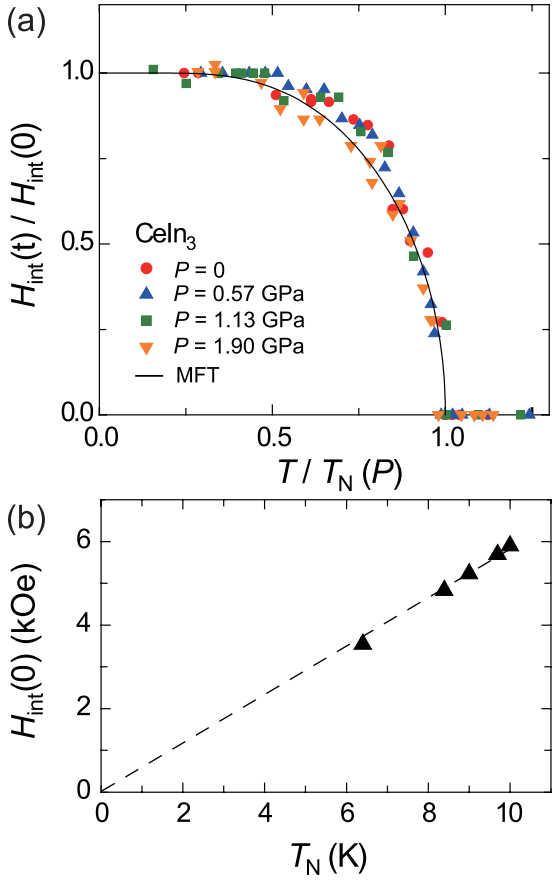

FIG. 4. (Color online) (a) Plots of $H_{int}(t)/H_{int}(0)$ vs $T/T_N(P)$ for the AFM phase. Here, $H_{int}(0)$ is a saturated value extrapolated to $T=0$. The solid curve indicates the molecular-field theory (MFT) with $S=1/2$. (b) $H_{int}(0)$ vs T_N plot in a P range of $P=0-1.90$ GPa. The dotted line is a guide to the eye.

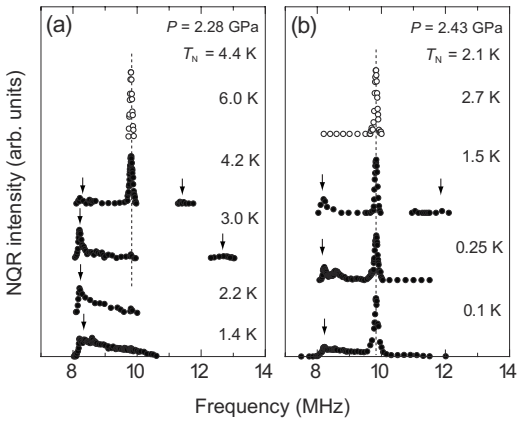

FIG. 5. Temperature dependence of the $1\nu_Q$-NQR spectrum at (a) $P=2.28$ and (b) $P=2.43$ GPa just below $P_c=2.46$ GPa. Open and solid circles indicate the respective spectra above and below T_N. The dotted line and solid arrows point to the respective frequencies where the peak in NQR spectrum is observed for the PM and AFM phases.

III. EVIDENCE FOR A PRESSURE-INDUCED FIRST-ORDER QUANTUM PHASE TRANSITION FROM ANTIFERROMAGNETISM TO PARAMAGNETISM

The P dependences of T_N and $H_{int} \propto M_{AFM}$ in the AFM phase are deduced from the analysis of the $3\nu_Q$ spectrum ($7/2 \Leftrightarrow 5/2$ transition) below T_N, which is significantly shifted below T_N, as denoted by the arrows in Fig. 3(b). Plots of $H_{int}(t)/H_{int}(0)$ vs $t=T/T_N(P)$ are presented for various P in Fig. 4(a). Here, $H_{int}(0)$ is a value at $T=0$. Significantly, the T dependence of M_{AFM} below T_N in a range of $P=0-2$ GPa is in good agreement with the molecular-field theory (MFT) with spin $S=1/2$ and $m_{AFM}=\tanh(m_{AFM}/t)$ as indicated by the solid curve in Fig. 4(a), reflecting a localized magnetic character of AFM in $CeIn_3$. It must be noted that in Fig. 4(b), $H_{int} \propto M_{AFM}$ is in proportion to T_N until $P \sim 2$ GPa.

Although T_N and $H_{int}(0)$ steeply decrease as P approaches P_c above 2 GPa, the T dependence of the $1\nu_Q$-NQR spectrum allows us to detect precisely the presence of an AFM order even in the vicinity of P_c. In fact, Figs. 5(a) and 5(b) show the T dependences of those at $P=2.28$ and 2.43 GPa where the respective spectra above and below T_N are indicated by open and solid symbols. It should be noted that the spectrum due to the PM phase is observed at 3 K and 0.1 K and even below $T_N=4.4$ K and 2.1 K at $P=2.28$ GPa and 2.43 GPa, respectively. This means that a phase separation into AFM and PM occurs as P approaches P_c. This result is corroborated by the P dependence of the spectra at temperatures lower than T_N, which are shown in the top, middle, and bottom parts of Fig. 6 for $P=2.37$, 2.43, and 2.50 GPa, respectively. Apparently, the phase separation into the AFM and PM phases occurs in the vicinity of P_c.

The NQR spectral intensity $I(T)$ increases with $1/T$ upon cooling, and $I(T) \times T$ is proportional to the number of observable In nuclei. Hence, the $I(T) \times T$ value for the NQR spectrum must be constant in the PM state. In fact, as shown in Fig. 7, where the data are normalized by a value at high temperatures above T_N at each P, $I(T) \times T$ remains a constant for $P=2.65$ GPa larger than P_c where the AFM order collapses. In contrast, the $I(T) \times T$ value decreases to zero upon cooling for $P=2.28$ and 2.32 GPa, which are lower than P_c. Unexpectedly, note that their decreasing behavior is not as steep below T_N, suggesting a possible distribution of T_N due to an inevitable distribution of P inside the sample. It is noteworthy that each $I(T) \times T$for $P=2.43$ and 2.50 GPa near P_c decreases due to the onset of the AFM order below T_N, but becomes constant below $T \sim 1.2$ K in both pressures and remains a finite value at the lowest temperatures; this is corroborated by the NQR spectra at $T=0.1$ K as indicated in Fig. 6. These results reveal that both the AFM and PM phases are mixed at $P=2.43$ and 2.50 GPa near P_c. Since T_N decreases steeply near P_c, this mixture is associated with an inevitable distribution of P inside the sample, revealing that the application of P is not always homogeneous.

Considering this experimental situation in mind, we attempt to reproduce the P dependences of the NQR spectra in Fig. 6, temperature dependence of $I(T) \times T$ in various pressures in Fig. 7, and the volume fraction of the AFM (V_{AFM}) in Fig. 8 by assuming the following Gaussian distribution of P inside the sample:

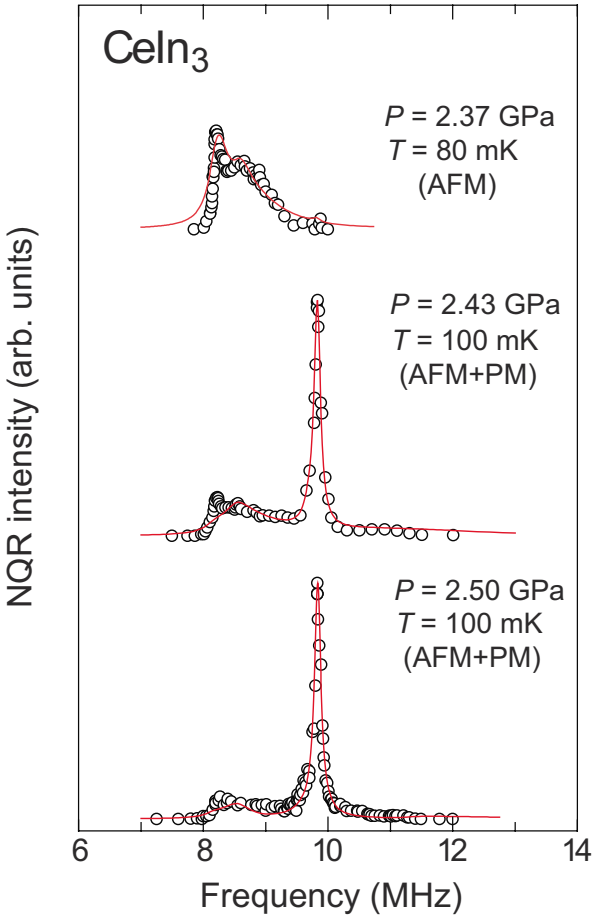

FIG. 6. (Color online) $1\nu_Q$-NQR spectra for $P=2.37$ and 2.43 GPa just below $P_c=2.46$ GPa and for $P=2.50$ GPa just above P_c. Solid curves are the simulations assuming an inevitable P distribution inside the sample in the pressure cell (see text). In the vicinity of P_c, NQR spectra result from the AFM and PM phases, which are separated by the first-order quantum phase transition. Here, the NQR spectral intensity is normalized by a peak intensity of the NQR spectrum of the PM phase.

$$V(P_0,P)=\frac{1}{\sqrt{2\pi}\sigma}\exp\left[-\frac{1}{2\sigma^2}(P-P_0)^2\right] \quad (1)$$

and

$$\int_{-\infty}^{\infty} V(P_0,P)dP=1 \quad (2)$$

Here, P_0 represents an external pressure and σ represents the mean deviation in the Gaussian distribution function. A P dependence of V_{AFM} is obtained by the integration of $V(P_0,P)$ against P from $-\infty$ to P_c as follows:

$$V_{\mathrm{AFM}}(P_0)=\int_{-\infty}^{P_c} V(P_0,P)dP. \quad (3)$$

Figure 8 shows the P dependence of V_{AFM}, which is determined by the NQR intensity at $T=0.1$ K (see Figs. 6 and 7). As shown in the solid curve in Fig. 8, a best fit to the data

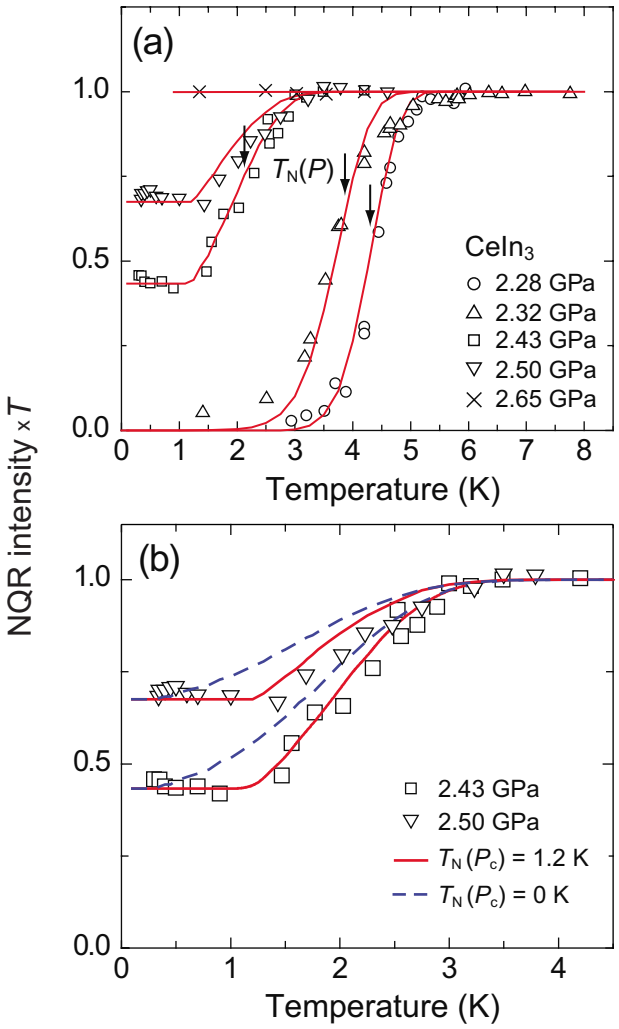

FIG. 7. (Color online) (a) Temperature dependence of the NQR intensity × temperature for the $1\nu_Q$ transition around P_c. Arrows indicate T_N at $P=2.28$, 2.32, and 2.43 GPa. The solid curve is a simulation assuming that T_N is distributed due to the inevitable P distribution in the pressure cell (see text). (b) Temperature dependence of NQR intensity × temperature at $P=2.43$ and 2.50 GPa. Solid and dotted curves are simulations assuming first-order $[T_N(P_c)=1.2\ \mathrm{K}]$ and second-order $[T_N(P_c)=0\ \mathrm{K}]$ phase transitions, respectively.

is obtained with parameters $\sigma=0.05$ and $P_c=2.46$ GPa. Here, a dotted line is drawn as a phase boundary at $T=0$ if a pressure distribution were absent. This *in situ* P distribution is comparable to the values in other experiments that were performed using a piston-cylinder-type clamping cell.[41,42] By using the above parameters of $\sigma=0.05$ and $P_c=2.46$ GPa, we show that the spectra in the range of $P=2.37-2.50$ GPa shown in Fig. 6 are consistently simulated by assuming that the T dependence of $H_{\mathrm{int}}(T)$, which is induced by AFM moments, can be described in terms of the molecular-field model and the relation $T_N \propto H_{\mathrm{int}}(0)$. Further, we assume the Pdependence of T_N as $T_N(P)=4.0\left(\frac{2.475-P}{2.475-2.31}\right)^{0.5}$ just below $P_c=2.46$ GPa. As a result, we have obtained excellent fittings, as shown by the solid lines in Figs. 6 and 7. Figure 9 indicates the thus obtained P dependence of T_N in $CeIn_3$.

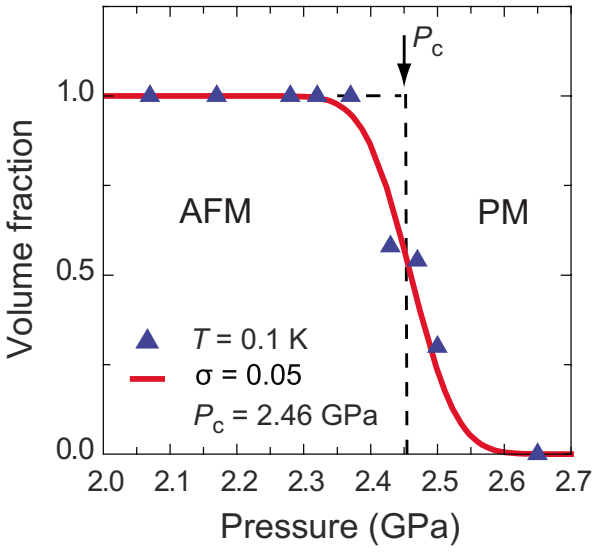

FIG. 8. (Color online) Pressure (P) dependence of the volume fraction of the AFM phase at $T=0.1$ K in the vicinity of P_c. The solid curve is a simulation assuming a Gaussian-type P distribution inside the sample in the P cell (see text). The vertical dotted line indicates the first-order quantum phase transition for $\sigma=0$ provided that a P distribution is absent. Arrow points to $P_c=2.46$ GPa.

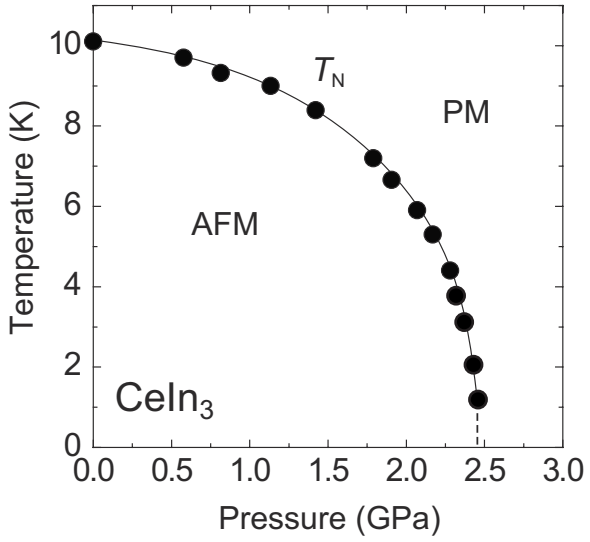

FIG. 9. Pressure dependence of T_N in $CeIn_3$. T_N above $P=2.28$ GPa are determined from the analysis of the T and P dependences of the NQR spectrum. The solid curve is a guide to the eye. Dotted line indicates $P_c=2.46$ GPa where the first-order quantum phase transition separates AFM and PM.

Remarkably, T_N disappears suddenly at a minimum value of $T_N=1.2$ K at $P_c=2.46$ GPa, suggesting a weak first-order QPT from AFM to PM in $CeIn_3$ as a function of P. Figure 7(b) shows the T dependences of $I(T)\times T$ at $P=2.43$ and 2.50 GPa and simulation curves assuming first-order phase transition with $T_N(P_c)=1.2$ K (solid curves) and second-order phase transition with $T_N(P_c)=0$ K (dotted curves), respectively. Notably, the simulation for second-order phase transition does not fit the experimental data at all. Especially, the $I(T)\times T=$const behavior below $T_N(P_c)=1.2$ K observed at $P=2.43$ and 2.50 GPa near P_c is a significant feature of first-order phase transitions. This contrasts with the phase diagram of the HF antiferromagnet $CeRhIn_5$ under P which is characterized by the tetracritical point separating the pure AFM phase, the uniformly coexisting phase of AFM+SC, and the PM-SC phase.[20]

IV. PRESSURE-INDUCED EVOLUTION OF MAGNETIC PROPERTIES AROUND P_c

Figure 10 shows the T dependences of $1/T_1$ [Fig. 10(a)] and $1/T_1T$ [Fig. 10(b)] in $CeIn_3$ at $P=0$, 1.79, 2.17, 2.43, and 2.65 GPa. The $1/T_1$ result at $P=0$ is consistent with the previous one.[32] $1/T_1$ at $P=0$ shows a gradual increase upon cooling and stays constant until T_N below 40 K, which evidences a localized nature of Ce-4f–derived magnetic fluctuations coupled with each other via the Ruderman-Kittel-Kasuya-Yosida (RKKY) interaction. Below T_N, $1/T_1$ decreases significantly without any critical slowing-down behavior near T_N. Similar behaviors were reported in $1/T_1$ in $CePd_2Si_2$.[43] In this compound, when noting that a Kondo temperature T_K is nearly the same as T_N, the absence of critical magnetic fluctuations towards T_N may be relevant to a competition between the Kondo local interaction and the RKKY intersite interaction. Notably, $1/T_1T$ remains constant well below T_N at low temperatures, probing a residual Fermi surface in the AFM state.

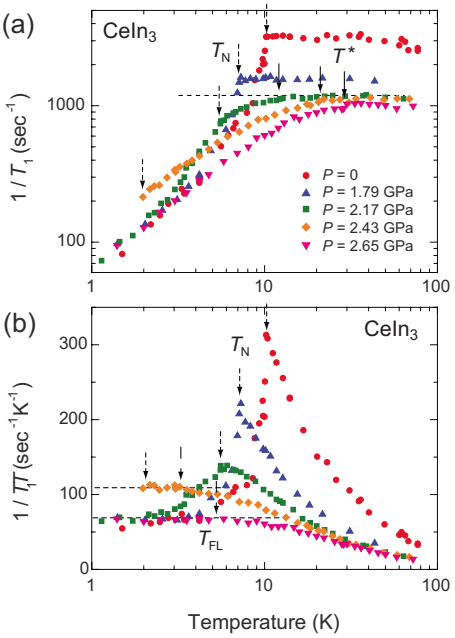

FIG. 10. (Color online) (a) Temperature dependence of $1/T_1$ at $P=0$, 1.79, 2.17, 2.43, and 2.65 GPa. The dotted line indicates a relation of $1/T_1=$const. Dotted and solid arrows point to T_N and T^*, respectively. (b) Temperature dependence of $1/T_1T$ at $P=0$, 1.79, 2.17, 2.43, and 2.65 GPa. The dotted line indicates the relation of $1/T_1T=$const. Dotted and dashed arrows indicate T_N and T_{FL}, respectively.

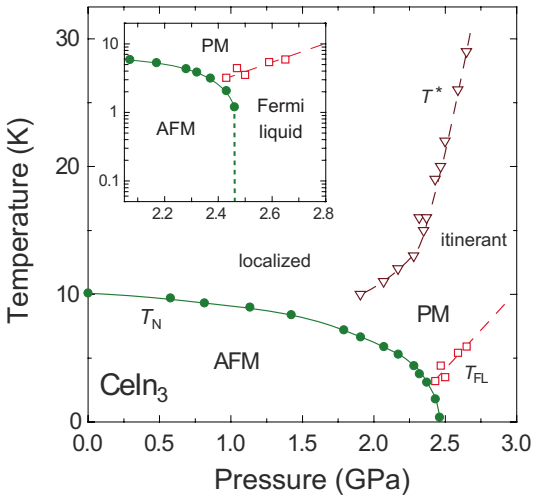

FIG. 11. (Color online) The P-T phase diagram of the magnetic properties for $CeIn_3$ obtained from the present NQR experiments. Solid circles indicate T_N, while open triangles denote a crossover temperature T^* from a localized to an itinerant regime of $4f$ electrons; open squares indicate a Fermi temperature T_{FL} below which a HF state is established. The inset shows the detailed phase diagram in the vicinity of P_c in a semilogarithmic scale. The vertical dotted line indicates the first-order phase boundary with a minimum value of $T_N=1.2$ K between the AFM and PM.

Next, we deal with the results under P. Since $1/T_1$ still remains constant just above T_N up to $P=1.79$ GPa, a localized magnetic character is robust against the application of P

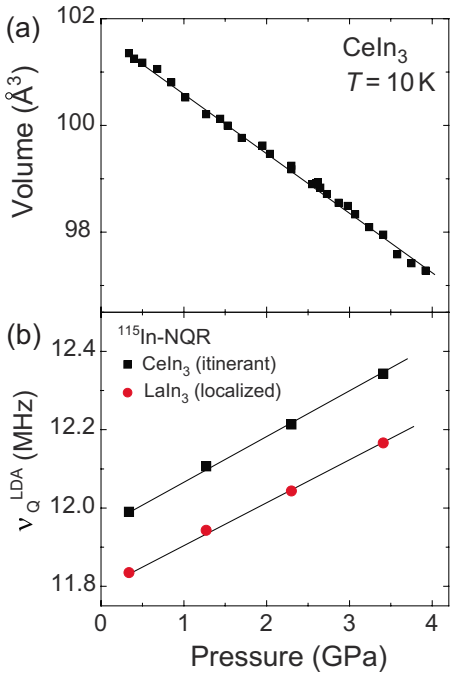

FIG. 12. (Color online) (a) Pressure dependence of the lattice volume for $CeIn_3$. (b) P dependence of ν_Q obtained from the local-density-approximation band calculation for $CeIn_3$ and $LaIn_3$. $LaIn_3$ corresponds to the $4f$-localized model of $CeIn_3$. Both are calculated with the same lattice constant.

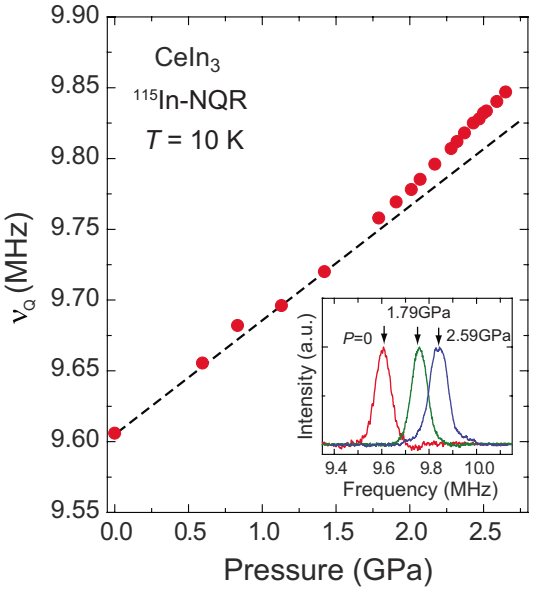

FIG. 13. (Color online) Pressure dependence of ν_Q at $T=10$ K. The dotted line is a guide to the eye. The inset shows $1\nu_Q$-NQR spectra at $P=0$, 1.79, and 2.59 GPa.

in $CeIn_3$. In a localized regime, $1/T_1$ is proportional to p_{eff}^2/J_{ex} or $\sim p_{eff}^2 W/J_{cf}^2$. Here p_{eff}, J_{ex}, J_{cf}, and W are an effective PM local moment, the RKKY exchange constant, the exchange constant between $4f$ moments and conduction-electron spins, and the bandwidth of conduction electrons, respectively. A progressive suppression of the value of $1/T_1=$constant at high temperatures with increasing P is considered to be due to a reduction in p_{eff} and/or an increase in J_{cf}. As a result, $1/T_1$ starts to decrease below $T^*=10$ K in a P range exceeding $P\sim 1.9$ GPa as observed in Fig. 10(a). In HF systems, it is known that T^* is scaled to the quasielastic linewidth in a neutron-scattering spectrum, leading to a tentative estimation of the bandwidth of the HF state. As shown in Fig. 11, as P exceeds P_c, T^* increases steeply up to $T^*\sim 30$ K at $P=2.65$ GPa.[37]

Figure 10(b) indicates the P and T dependences of $1/T_1T$ that probes low-lying excitations in an itinerant regime. Notably, a behavior that $1/T_1T=$const is observed below $T_{FL}=3.2$ K at $P=2.43$ GPa just below $P_c=2.46$ GPa. Here, we defined T_{FL} as a Fermi temperature below which $1/T_1T$ becomes constant. As shown in the inset of Fig. 11, the HF state is realized below $T_{FL}=3.2$ K at $P=2.43$ GPa, which is just below P_c. Remarkably, $T_N\sim 1.2$ K is lower than $T_{FL}\sim 4.5$ K at P_c. The HF-PM state and the AFM state compete to trigger the weakly first-order QPT at $P_c=2.46$ GPa in the case of $CeIn_3$. The P dependence of T_{FL} is in good agreement with the observation of T^2 dependence in resistivity measurements.[10] Non-Fermi-liquid behaviors due to the development of AFM spin fluctuations are not evident; one reason is that the HF state is already realized in the PM state above T_N just below P_c, and subsequently, a first-order QPT occurs near P_c.

Even though T_N is markedly decreased in the vicinity of P_c, being lower than T_{FL} above $P=2.43$ GPa, which suggests

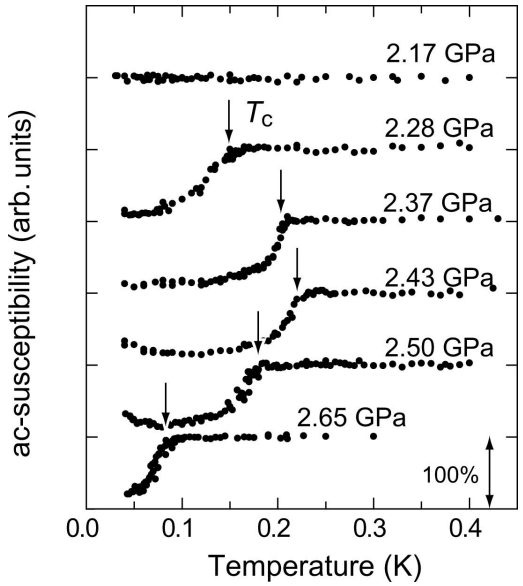

FIG. 14. Temperature dependence of χ_{ac} in a P range of 2.17–2.65 GPa. Arrows indicate an onset temperature T_c^{onset} below which SC diamagnetism starts to appear.

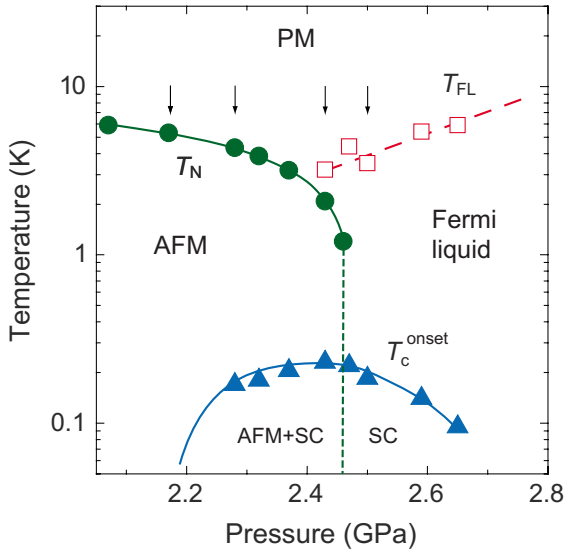

FIG. 15. (Color online) Detailed P-T phase diagram for PM, AFM, and SC for $CeIn_3$ in the vicinity of the first-order QPT at P_c=2.46 GPa, which is denoted by a vertical dashed line. Solid circles and triangles indicate T_N and T_c, respectively. The open square is a crossover temperature towards the HF state. T_c^{onset} is determined by χ_{ac} in a P range of 2.17–2.65 GPa. Arrows point to P=2.17, 2.28, 2.43, and 2.50 GPa where the $1/T_1$ shown in Fig. 16 was measured (see text).

an itinerant-type AFM order, we have suggested that as far as AFM order survives, a localized character is robust against closely approaching P_c. This is because the T dependences of NQR spectra and their spectral intensity near P_c are consistently simulated by assuming a localized character for AFM order. This robustness of the localized nature of AFM order just below P_c may be relevant with the first-order nature of QPT taking place at P_c.

V. ELECTRONIC STATE BEHIND THE FIRST-ORDER TRANSITION

Here, we characterize the first-order magnetic phase transition from the AFM to PM. An NQR frequency ν_Q probes the electric-field gradient (EFG) generated by the electron distribution surrounding the In site. In general, a compression of the lattice volume V increases ν_Q; i.e., ν_Q is proportional to $1/V$. In addition to this lattice contribution of EFG, a local electronic charge distribution at the In site generates an electronic contribution of EFG. While the lattice volume of $CeIn_3$ is actually compressed as P increases, as shown in Fig. 12(a), ν_Q estimated from the LDA band calculation increases for $CeIn_3$; an identical trend is obtained for $LaIn_3$, as shown in Fig. 12(b). Note that ν_Q for $CeIn_3$ is larger than that for $LaIn_3$. This is considered to be due to the electronic contribution of the EFG for $CeIn_3$ that originates from the hybridization between Ce-derived $4f$ electrons and p electrons at the In site. Figure 13 shows the P dependence of the NQR frequency and the ν_Q value at T=10 K. Here, the NQR spectra with P, which are displayed in the inset of Fig. 13, are obtained by the Fourier-transform method of the spin-echo signal. As observed in Fig. 13, in a lower-P region, the compression of the lattice volume increases ν_Q linearly. As P increases beyond 2 GPa where T^* starts to increase, ν_Q begins to increase significantly. The origin of a larger increasing rate of ν_Q at pressures larger than 2 GPa is due to the increase in the electric contribution that is related to the significant increase in hybridization between f electrons and conduction electrons. As a result, T_N decreases steeply with an increase in P. Notably, such a variation from a localized to an itinerant nature of the f electrons around P_c is also reported by the recent de Haas–van Alphen (dHvA) measurement under P.[44]

VI. PRESSURE-INDUCED SUPERCONDUCTIVITY AROUND P_c

In this section, the P-induced superconductivity in $CeIn_3$ is considered. Figure 14 shows the T dependence of the ac susceptibility χ_{ac} of $CeIn_3$ measured by an *in situ* NQR coil under P. In the range P=2.28–2.65 GPa, a clear decrease in χ_{ac} implies a SC transition under P. However, SC does not occur at P=2.17 GPa until T=30 mK, as can be noticed from the T independence of χ_{ac} shown in Fig. 14. Thus, a critical pressure P_{SC} for the onset of SC is between P=2.17 and 2.28 GPa. The absolute value of $\chi_{ac}$was corrected by a value of χ_{ac} measured on a single crystal of $CeIrIn_5$ in which bulk SC is fully established.[45] Figure 15 shows a SC phase diagram as the function of P. The P-induced SC emerges in the vicinity around P_c where the first-order transition occurs. This SC phase for $CeIn_3$ is consistent with other experiments.[5,10,19,44] It must be noted that the SC volume fraction is almost unchanged in the range P=2.28–2.65 GPa. Thus, the coexistence of AFM and SC is strongly indicative of a P range of P=2.28–2.46 GPa.

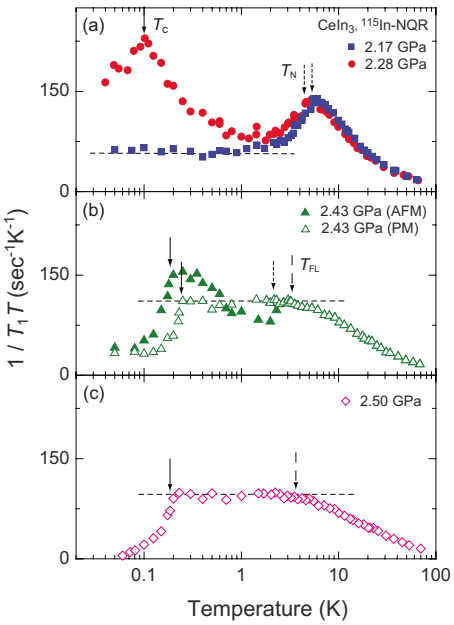

FIG. 16. (Color online) Temperature dependence of $^{115}(1/T_1T)$ for $CeIn_3$ at (a) $P=2.17$ and 2.28 GPa, (b) 2.43 GPa, and (c) 2.50 GPa. Open and solid symbols indicate the respective data for PM and AFM (see the text). The solid arrows indicate the respective SC transition temperature T_c^{PM} and T_c^{AFM} for PM and AFM. The dotted and dashed arrows indicate T_N and T_{FL} below which the HF state becomes valid, characterized by the T_1T=const law (dotted line).

VII. EVIDENCE FOR THE UNIFORMLY COEXISTING PHASE OF ANTIFERROMAGNETISM AND UNCONVENTIONAL SUPERCONDUCTIVITY

The coexistence of AFM and SC is directly evidenced from the T dependence of $1/T_1T$, which can probe low-lying excitations due to the quasiparticles in SC and also due to magnetic excitations in AFM. Figures 16(a)–16(c) show drastic changes in the T dependence of $1/T_1T$ at (a) $P=2.17$ and 2.28, (b) $P=2.43$ GPa, and (c) $P=2.50$ GPa, respectively. Each pressure is indicated by the arrow in Fig. 15. Note that since $P=2.43$ GPa is very close to $P_c=2.46$ GPa where the first-order transition occurs, the $1/T_1T$'s for PM and AFM are separately measured on the respective NQR spectral peaks (see the middle spectrum in Fig. 6), as shown in Fig. 16(b). Here, T_c is determined as a temperature below which $1/T_1T$ decreases significantly due to the SC gap opening, and the NQR intensity begins to decrease due to the Meissner shielding of rf pulses. Since the coherence peak is absent just below T_c, it suggests that unconventional superconductivity is induced in $CeIn_3$ under pressure. These results give microscopic evidence for the uniformly coexisting phase of the AFM and SC in the range $P=2.28-2.43$ GPa for $CeIn_3$. We note here that the behavior of $1/T_1T$=const observed at $P=2.37$ GPa [see Fig. 19(a)] reveals that the SC phase in the AFM+SC uniformly coexisting state does not exhibit a line-node gap, but is in a gapless regime. This is in contrast with the SC phase in the PM phase at $P=2.50$ GPa where the T^3 dependence of $1/T_1$ is observed as discussed later.

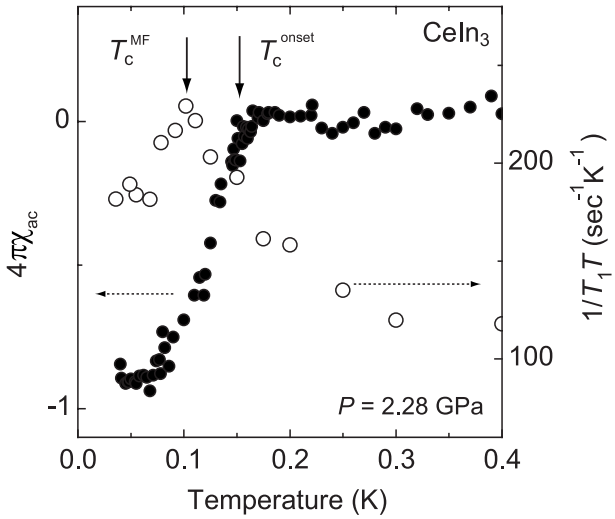

FIG. 17. Temperature dependence of $^{115}(1/T_1T)$ (open circles) and χ_{ac} (solid circles) for $CeIn_3$ at $P=2.28$ GPa where the SC emerges. Arrows point to T_c^{MF} below which $^{115}(1/T_1T)$ decreases and T_c^{onset} below which the SC diamagnetism appears.

Figure 17 demonstrates the SC characteristics for the coexistence of AFM and SC at $P=2.28$ GPa. Below $T=3$ K, $1/T_1T$ continues to increase moderately down to $T_c^{MF}=0.1$ K even though it crosses $T_c^{onset}\sim 0.15$ K. This relaxation behavior suggests that the SC order parameter does not always develop below T_c^{onset}. These characteristics for the uniformly coexisting phase of the AFM and SC are similar to those for the P-induced superconductor $CeRhIn_5$.[22,20] Noting that T_c^{MF} coincides with T_c^{onset} at $P=2.65$ GPa with $T_c=95$ mK,[29] the difference between T_c^{MF} and T_c^{onset}at $P=2.28$ GPa is not due to the P distribution but due to the uniform coexistence of the AFM and SC.

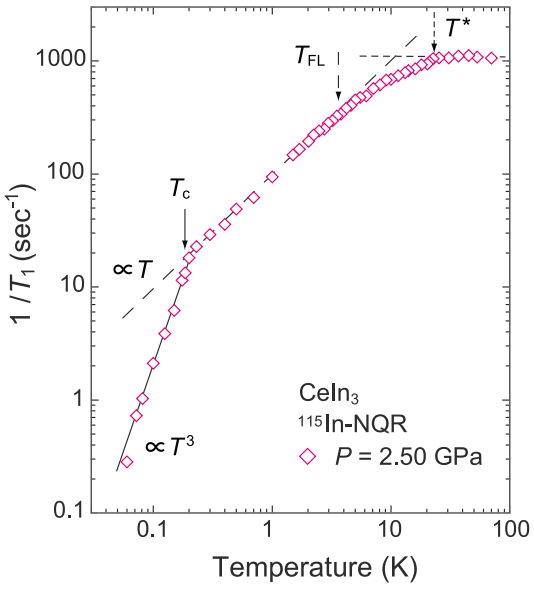

FIG. 18. (Color online) Temperature dependence of $1/T_1$ at $P=2.50$ GPa just above $P_c=2.46$ GPa. Solid, dashed, and dotted arrows indicate T_c, T_{FL}, and T^*, respectively. Solid, dashed, and dotted lines indicate the respective relations of $1/T_1\propto T^3$, $1/T_1\propto T$, and $1/T_1$=const.

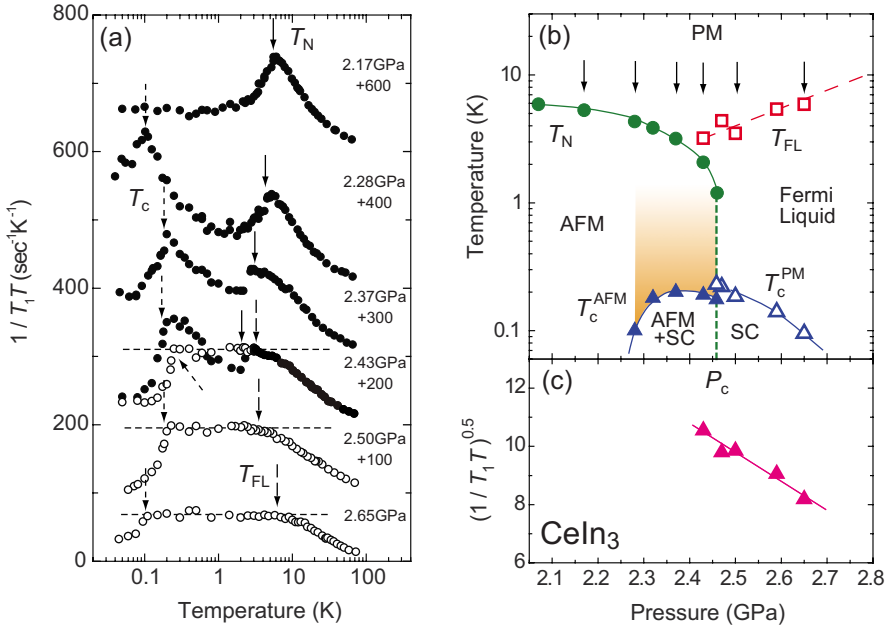

FIG. 19. (Color online) (a) Temperature dependences of $1/T_1T$ in a range $P=2.17-2.65$ GPa. The $1/T_1T$ data are offset for clarity. The solid and open symbols indicate the respective data of $1/T_1T$ measured below and above P_c. Solid, dotted, and dashed arrows indicate T_N, T_c, and T_{FL}, respectively. Dotted lines indicate a relation of $1/T_1T=$const. (b) The detailed P-T phase diagram of $CeIn_3$ in the vicinity of P_c. Shaded region indicates the unconventional magnetic state where the low-lying spin-density fluctuations develop down to T_c upon cooling. All these phases of matter are determined by the present NQR measurements under P (see text). The arrow points to a value of P where $1/T_1T$ in (a) was measured. (c) Pressure dependence of $(1/T_1T)^{0.5}$ for $P_c<P$ which is in proportion to the effective density of states at the Fermi level of HF band. Solid line is a guide to the eye.

Next, we focus on the novel low-lying magnetic excitations inside AFM. As shown in Fig. 16(a), the $1/T_1T=$const behavior is observed well below $T_N=5.3$ K at $P=2.17$ GPa as well as at $P=0$.[32,33] Unexpectedly, $1/T_1T$ at $P=2.28$ GPa, where T_N starts to steeply decrease, continues to increase upon cooling below T_N and exceeds the value at $T_N=4.4$ K regardless of AFM spin polarization being induced. This behavior is also observed in the AFM state at $P=2.37$ and 2.43 GPa, as shown in Figs. 16(b) and 19(a), respectively. Since $1/T_1T$ probes any type of low-lying excitations, it is probable that low-lying longitudinal spin-density fluctuations are responsible for this feature in association with the first-order QPT. This is because when the AFM critical temperature is suppressed at the termination point of the first-order QPT; i.e., when $P_c=2.46$ GPa, the diverging AFM spin-density fluctuations emerge at a critical point from AFM to PM. Namely, since a free energy of the system in the vicinity of P_c becomes almost the same between the AFM phase with a finite spin polarization at frequencies ($\omega\sim 0$) lower than an NMR frequency and the PM-HF state which does not carry static spin polarization but is dominated by low-lying excitations, it is likely that an amplitude of spin density is fluctuating in the vicinity of P_c. In this context, the P-induced SC in $CeIn_3$ does not always occur with the background of a magnetically soft-electron liquid state,[5] but instead, magnetic excitations, such as AFM spin density fluctuations relevant to a first-order transition from AFM to PM, might mediate an attractive interaction. Irrespective of the pairing mechanism being at $P=2.28$ GPa where AFM order is realized over the entire sample below $T=3$ K (see Fig. 7), the clear decrease in $1/T_1T$ and χ_{ac} provides convincing evidence for the uniformly coexisting phase of AFM and SC in $CeIn_3$. These results suggest that the P-induced SC in the AFM phase is closely related to the enhancement of hybridization that triggers the QPT from AFM to PM.

Significantly, the SC coexisting with AFM in $CeIn_3$ is reasonably unique as expected from the results at $P=2.43$ GPa, as shown in Fig. 16(b). At temperatures lower than the respective values of $T_c^{PM}=230$ mK and $T_c^{AFM}=190$ mK for PM and AFM phases, unexpectedly, the magnitudes of $1/T_1T=$const coincide with one another; nevertheless, both phases are separated across P_c where the first-order QPT occurs and the values of T_c differ. This means that the low-lying excitations may be identical in origin for the uniformly coexisting state of AFM+SC and for the PM+SC. How does this happen? It may be possible that both phases are in a dynamically separated regime with time scales smaller than the inverse of NQR frequency in order to make each SC phase for AFM and PM uniform across P_c. In this context, the observed magnetically separated phases and the relevant SC coexisting with AFM may belong to new phases of matter.

VIII. HEAVY-FERMION SUPERCONDUCTIVITY

Finally, we present evidence for the P-induced unconventional HF SC emerging at the PM phase beyond P_c where the low-lying AFM spin fluctuations are absent. This is because, as observed in Fig. 18, $1/T_1T=$const behavior is obeyed at

the normal state and $1/T_1$ follows a T^3 dependence below $T_c=185$ mK without the coherence peak just below T_c; this is consistent with the line-node gap model characteristic for an unconventional HF SC.[1,3,17,29,30,46–50] As observed in Fig. 19(a), the respective Fermi-liquid temperatures T_{FL} at $P=2.50$ GPa and $P=2.65$ GPa are defined as $T_{FL}=3.5$ K and 5.9 K, respectively; below this temperatures, the $1/T_1T=$const behavior is valid. Noting that the value of $(1/T_1T)^{1/2}$ is proportional to the effective density of state at the Fermi level, the value of $(1/T_1T)^{1/2}$ has a maximum at P_c where T_c has the maximum value of $T_c^{max}=230$ mK as observed in Fig. 19(c). This means that as an effective HF bandwidth becomes smaller and the system approaches P_c, T_c is increased up to the maximum value. This result reveals that the P-induced SC in $CeIn_3$ is realized under a strong electron correlation, although the antiferromagnetic QCP is absent. In this context, the first-order QPT plays an important role for the onset of unconventional HF SC as well.

IX. CONCLUSION

Extensive ^{115}In-NQR studies conducted under P on $CeIn_3$ have revealed the evolution of magnetic properties and P-induced unconventional SC characteristics as follows.

(i) The P-induced transition from AFM to PM is the first-order QPT at a critical pressure $P_c=2.46$ GPa at which the AFM order disappears with a minimum value of $T_N(P_c)=1.2$ K.

(ii) The hybridization between $4f$ electrons and conduction electrons increases beyond $P=2$ GPa, thereby stabilizing the HF-PM state. It is this competition between the AFM phase, where T_N is reduced, and the formation of the HF-PM phase that triggers the first-order QPT at $P_c=2.46$ GPa.

(ii) Despite the lack of an AFM QCP in the P-T phase diagram, unconventional SC occurs in both phases of AFM and PM. As a result, the AFM order uniformly coexists with the SC order.

(iv) The significant increase in $1/T_1$ upon cooling in the AFM phase has revealed the development of low-lying magnetic excitations until T_c, and this is related to the onset of the uniformly coexisting phase of SC+AFM.

(v) In the HF-PM phase where AFM spin fluctuations are absent, $1/T_1$ decreases without the coherence peak just below T_c, followed by a power-law-like T dependence that indicates an unconventional SC with a line-node gap.

(vi) T_c has a peak around P_c in the HF-paramagnetic phase as well as in the AFM phase and an SC dome exists with a maximum value of $T_c=230$ mK around P_c. These results suggest that the origin for the P-induced HF SC in $CeIn_3$ is *not related to the AFM spin fluctuations but is related to the emergence of the first-order QPT* at $P_c=2.46$ GPa.

These phenomena observed in $CeIn_3$ should be understood in terms of the first-order QPT because these new phases of matter are induced by applying P. When the AFM critical temperature is suppressed at the termination point of the first-order QPT—i.e., when $P_c=2.46$ GPa—it is anticipated that the diverging AFM spin-density fluctuations emerge at the critical point from AFM to PM. The results on $CeIn_3$ leading to a new type of quantum criticality deserve further theoretical investigations.

ACKNOWLEDGMENTS

S. K. thanks Yuki Fuseya and Shinji Watanabe for their valuable discussions, comments, and encouragement. S.K. also thanks T. Mito, A.V. Kornilov, C. Thessieu, Y. Kawasaki, H. Kotegawa, K. Ishida, T. Muramatsu, J. Flouquet, and G.-q. Zheng for their assistance during the experiments and/or useful discussions during the early stage of this work. This work was supported by a Grant-in-Aid for Creative Scientific Research (Grant No. 15GS0213), MEXT, and The 21st Century COE Program supported by the Japan Society for the Promotion of Science. The synchrotron radiation experiments were performed at BL10XU in SPring-8 with the approval of the Japan Synchrotron Radiation Research Institute (Proposal No. 2001A0004-LD -np).

*Present address: Department of Physics, Faculty of Science, Okayama University, Okayama 700-8530, Japan. kawasaki@science.okayama-u.ac.jp

†Present address: Department of Physics, Graduate School of Science, Kyoto University, Kyoto 606-8502, Japan.

[1] For review see, Y. Kuramoto and Y. Kitaoka, *Dynamics of Heavy Electrons* (Oxford University Press, Oxford, 2000), and references therein.

[2] F. Steglich, J. Aarts, C. D. Bredl, W. Lieke, D. Meschede, W. Franz, and H. Schafer, Phys. Rev. Lett. **43**, 1892 (1979).

[3] Y. Kitaoka, S. Kawasaki, T. Mito, and Y. Kawasaki, J. Phys. Soc. Jpn. **74**, 186 (2005).

[4] J. Bardeen, L. N. Cooper, and J. R. Schrieffer, Phys. Rev. **108**, 1175 (1957).

[5] N. D. Mathur, F. M. Grosche, S. R. Julian, I. R. Walker, D. M. Freye, R. K. W. Haselwimmer, and G. G. Lonzarich, Nature (London) **394**, 39 (1998).

[6] F. M. Grosche, S. R. Julian, N. D. Mathur, and G. G. Lonzarich, Physica B **223 & 224**, 50 (1996).

[7] F. M. Grosche, I. R. Walker, S. R. Julian, N. D. Mathur, D. M. Freye, M. J. Steiner, and G. G. Lonzarich, J. Phys.: Condens. Matter **13**, 2845 (2001).

[8] I. R. Walker, F. M. Grosche, D. M. Freye, and G. G. Lonzarich, Physica C **282-287**, 303 (1997).

[9] T. Muramatsu, Ph. D thesis, Osaka University, 2001.

[10] G. Knebel, D. Braithwaite, P. C. Canfield, G. Lapertot, and J. Flouquet, Phys. Rev. B **65**, 024425 (2001).

[11] S. Kawasaki, T. Mito, Y. Kawasaki, H. Kotegawa, G.-q. Zheng, Y. Kitaoka, H. Shishido, S. Araki, R. Settai, and Y. Ōnuki, J. Phys. Soc. Jpn. **73**, 1647 (2004).

[12] R. Movshovich, T. Graf, D. Mandrus, J. D. Thompson, J. L. Smith, and Z. Fisk, Phys. Rev. B **53**, 8241 (1996).

[13] S. Araki, M. Nakashima, R. Settai, T. C. Kobayashi, and Y. Ōnuki, J. Phys.: Condens. Matter **14**, L377 (2002).
[14] B. Bellarbi, A. Benoit, D. Jaccard, J.-M. Mignot, and H. F. Braun, Phys. Rev. B **30**, 1182 (1984).
[15] F. Thomas, J. Thomasson, C. Ayache, C. Geibel, and F. Steglich, Physica B **186-188**, 303 (1993).
[16] Y. Kawasaki, K. Ishida, T. Mito, C. Thessieu, G.-q. Zheng, Y. Kitaoka, C. Geibel, and F. Steglich, Phys. Rev. B **63**, 140501(R) (2001).
[17] Y. Kawasaki, K. Ishida, S. Kawasaki, T. Mito, G.-q. Zheng, Y. Kitaoka, C. Geibel, and F. Steglich, J. Phys. Soc. Jpn. **73**, 194 (2004).
[18] H. Hegger, C. Petrovic, E. G. Moshopoulou, M. F. Hundley, J. L. Sarrao, Z. Fisk, and J. D. Thompson, Phys. Rev. Lett. **84**, 4986 (2000).
[19] T. Muramatsu, N. Tateiwa, T. C. Kobayashi, K. Shimizu, K. Amaya, D. Aoki, H. Shishido, Y. Haga, and Y. Ōnuki, J. Phys. Soc. Jpn. **70**, 3362 (2001).
[20] M. Yashima, S. Kawasaki, H. Mukuda, Y. Kitaoka, H. Shishido, R. Settai, and Y. Ōnuki, Phys. Rev. B **76**, 020509(R) (2007).
[21] T. Mito, S. Kawasaki, Y. Kawasaki, G.-q. Zheng, Y. Kitaoka, D. Aoki, Y. Haga, and Y. Ōnuki, Phys. Rev. Lett. **90**, 077004 (2003).
[22] S. Kawasaki, T. Mito, Y. Kawasaki, G.-q. Zheng, Y. Kitaoka, D. Aoki, Y. Haga, and Y. Ōnuki, Phys. Rev. Lett. **91**, 137001 (2003).
[23] H. Q. Yuan, F. M. Grosche, M. Deppe, C. Geibel, G. Sparn, and F. Steglich, Science **302**, 2104 (2003).
[24] Y. Onishi and K. Miyake, J. Phys. Soc. Jpn. **69**, 3955 (2000).
[25] K. Miyake and H. Maebashi, J. Phys. Soc. Jpn. **71**, 1007 (2002).
[26] S. Watanabe, M. Imada, and K. Miyake, J. Phys. Soc. Jpn. **75**, 043710 (2006).
[27] P. G. Pagliuso, C. Petrovic, R. Movshovich, D. Hall, M. F. Hundley, J. L. Sarrao, J. D. Thompson, and Z. Fisk, Phys. Rev. B **64**, 100503(R) (2001).
[28] M. Nicklas, V. A. Sidorov, H. A. Borges, P. G. Pagliuso, J. L. Sarrao, and J. D. Thompson, Phys. Rev. B **70**, 020505(R) (2004).
[29] S. Kawasaki, G.-q. Zheng, H. Kan, Y. Kitaoka, H. Shishido, and Y. Ōnuki, Phys. Rev. Lett. **94**, 037007 (2005).
[30] S. Kawasaki, M. Yashima, Y. Mugino, H. Mukuda, Y. Kitaoka, H. Shishido, and Y. Ōnuki, Phys. Rev. Lett. **96**, 147001 (2006).
[31] P. Morin, C. Vettier, J. Flouquet, M. Konczykowski, Y. Lassailly, J.-M. Mignot, and U. Welp, J. Low Temp. Phys. **70**, 377 (1988).
[32] Y. Kohori, Y. Inoue, T. Kohara, G. Tomka, and P. C. Riedi, Physica B **259-261**, 103 (1999).
[33] Y. Kohori, T. Kohara, Y. Yamato, G. Tomka, and P. C. Riedi, Physica B **281-282**, 12 (2000).
[34] W. Knafo, S. Raymond, B. Fak, G. Lapertot, P. C. Canfield, and J. Flouquet, J. Phys.: Condens. Matter **15**, 3741 (2003).
[35] For a review, see T. Moriya and K. Ueda, Adv. Phys. **49**, 555 (2000), and references therein.
[36] C. Thessieu, K. Ishida, S. Kawasaki, T. Mito, Y. Kawasaki, G.-q. Zheng, Y. Kitaoka, and Y. Ōnuki, Physica B **281-282**, 9 (2000).
[37] S. Kawasaki, T. Mito, G.-q. Zheng, C. Thessieu, Y. Kawasaki, K. Ishida, Y. Kitaoka, T. Muramatsu, T. C. Kobayashi, D. Aoki, S. Araki, Y. Haga, R. Settai, and Y. Ōnuki, Phys. Rev. B **65**, 020504(R) (2001).
[38] S. Kawasaki, T. Mito, Y. Kawasaki, G.-q. Zheng, Y. Kitaoka, H. Shishido, S. Araki, R. Settai, and Y. Ōnuki, Phys. Rev. B **66**, 054521 (2002).
[39] A. S. Kirichenko, A. V. Kornilov, and V. M. Pudalov, Instrum. Exp. Tech. **48**, 121 (2005).
[40] F. Izumi and T. Ikeda, Mater. Sci. Forum **321-324**, 198 (2000).
[41] Y. Kawasaki, K. Ishida, T. Mito, C. Thessieu, G.-q. Zheng, Y. Kitaoka, C. Geibel, and F. Steglich, Phys. Rev. B **63**, 140501(R) (2001).
[42] G. Knebel, M.-A. Measson, B. Salce, D. Aoki, D. Braithwaite, J. P. Brison, and J. Flouquet, J. Phys.: Condens. Matter **16**, 8905 (2004).
[43] Y. Kawasaki, K. Ishida, Y. Kitaoka, and K. Asayama, Phys. Rev. B **58**, 8634 (1998).
[44] R. Settai, T. Kubo, T. Shiromoto, D. Honda, H. Shishido, K. Sugiyama, Y. Haga, T. D. Matsuda, K. Betsuyaku, H. Harima, T. C. Kobayashi, and Y. Ōnuki, J. Phys. Soc. Jpn. **74**, 3016 (2005).
[45] A. Sumiyama, D. Katayama, Y. Oda, Y. Inada, D. Aoki, Y. Tokiwa, Y. Haga, and Y. Ōnuki, J. Phys.: Condens. Matter **13**, L879 (2001).
[46] K. Ishida, Y. Kawasaki, K. Tabuchi, K. Kashima, Y. Kitaoka, K. Asayama, C. Geibel, and F. Steglich, Phys. Rev. Lett. **82**, 5353 (1999).
[47] T. Mito, S. Kawasaki, G.-q. Zheng, Y. Kawasaki, K. Ishida, Y. Kitaoka, D. Aoki, Y. Haga, and Y. Ōnuki, Phys. Rev. B **63**, 220507(R) (2001).
[48] G.-q. Zheng, K. Tanabe, T. Mito, S. Kawasaki, Y. Kitaoka, D. Aoki, Y. Haga, and Y. Ōnuki, Phys. Rev. Lett. **86**, 4664 (2001).
[49] Y. Kawasaki, S. Kawasaki, M. Yashima, T. Mito, G.-q. Zheng, Y. Kitaoka, H. Shishido, R. Settai, Y. Haga, and Y. Ōnuki, J. Phys. Soc. Jpn. **72**, 2308 (2003).
[50] M. Yashima, S. Kawasaki, Y. Kawasaki, G.-q. Zheng, Y. Kitaoka, H. Shishido, R. Settai, Y. Haga, and Y. Ōnuki, J. Phys. Soc. Jpn. **73**, 2073 (2004).